D band Raman intensity calculation in armchair edged graphene nanoribbons

E. B. Barros, K. Sato, Ge. G. Samsonidze, A. G. Souza Filho, M. S. Dresselhaus, and R. Saito

Phys. Rev. B **83**, 245435 — Published 27 June 2011

DOI: 10.1103/PhysRevB.83.245435

D band Raman intensity calculation in armchair edged graphene nanoribbons

E. B. Barros[1,2,*] K. Sato[2], Ge. G. Samsonidze[3], A. G. Souza Filho[1], M. S. Dresselhaus[4], and R. Saito[2]
[1] *Departamento de Física, Universidade Federal do Ceará, Fortaleza, Ceará, 60455-760 Brazil.*
[2] *Department of Physics, Tohoku University, Sendai 980-8578, Japan.*
[3] *Department of Physics, University of California at Berkeley, and Materials Sciences Division, Lawrence Berkeley National Laboratory, Berkeley, CA 94720*
[4] *Department of Electrical Engineering and Computer Science and Department of Physics, Massachusetts Institute of Technology, Cambridge, MA, 02139-4307 USA.*
(Dated: May 3, 2011)

The D band Raman intensity is calculated for armchair edged graphene nanoribbons using an extended tight-binding method, in which the effect of interactions up to the 7^{th} nearest neighbor is taken into account. The possibility of a double resonance Raman process with multiple scattering events is considered by calculating a T-matrix through a direct diagonalization of the nanoribbon Hamiltonian. We show that long range interactions play an important role in the evaluation of both the D band intensity and that the main effect of multiple scattering events on the calculated D band is an overall increase in intensity by a factor of four. The D band intensity is shown to be independent of the nanoribbon widths for widths larger than 17 nm, leading to the well known linear dependence of the I_D/I_G ratio on the inverse of the crystallite size. The D band intensity was shown to be nearly independent of the laser excitation energy and to have a maximum value for incident and scattering photons polarized along the direction of the edge.

PACS numbers:

1. INTRODUCTION

The D-band Raman spectra in both graphene and single wall carbon nanotubes (SWNTs) has been widely used to characterize defective carbon-based samples. It has been known that the D band intensity depends both on the crystallite size and on the laser excitation energy ($E_{\rm laser}$) in such a way that the D band intensity is inversely proportional to the in-plane crystaline size[1,2] (for d larger than 20 nm) and the D band to G band relative intensity (I_D/I_G) is proportional to $E_{\rm laser}^{-4}$.[2] Experimental evidence suggests that the main dependence of the I_D/I_G ratio on the laser excitation originates mainly from an increase in the I_G intensity with increasing laser excitation energy as $I_G = E_{\rm laser}^4$ while the D band intensity I_D would be mainly independent of the laser excitation energy.[3] A recent independent experimental work by Narula *et al.*[4] investigating the Raman scattering matrix elements of the D and G bands observed that the D band intensity increases nearly linearly with laser excitation for graphene ($E_{\rm laser} < 2.6$ eV). Also, different $E_{\rm laser}$ dependences were found for the D and G band intensities for monolayer graphene on Si/SiO_2 and pencil graphite.[4] Furthermore, Sasaki *et al.* have studied the polarization dependence of the D band intensity for nanoribbons, observing that the D band intensity has a maximum when both the incident and the scattered photons are polarized along the direction of the armchair edge.[5]

The D band intensity is usually explained considering a double resonance Raman scattering (DRRS) mechanism[6,7] in which the defect acts as an elastic scatterer for the photo-excited electron in the second-order scattering processes in k space. In order to estimate the role of the defect on the double resonance process, it is necessary to calculate the elastic scattering amplitude between two k states in the Brillouin zone. Formally, the scattering amplitude for a given scattering potential can be expressed by the so-called T matrix, in which the modification of the electronic states by scattering is taken into account in an infinite series expansion.[8] Sato *et al.* calculated the D band intensity for armchair-edged graphene ribbons in which they consider the first-order term of the scattering matrix and they obtained a dependence for the D band integrated intensity on $E_{\rm laser}$.[9] In the previous calculation, the electron-defect scattering matrix elements were obtained within a simple tight-binding method (STB) for the nearest-neighbor atoms in which the scattering at an armchair edge is taken into account as missing transfer integrals of the nearest neighbor atoms at the edges.

Although these approximations can give insight into the overall properties of the D-band Raman peak, the modification of the electronic wave functions by the scattering wave was not considered by higher order terms in the perturbation expansion. Furthermore, in the previous calculation, we considered only the first nearest neighbor interactions for the scattering potential which does not always represent the full range of the scattering potential.

In the present paper we will evaluate both of these missing effects by considering farther neighbors and by considering the effect of multiple scattering processes on the total elastic scattering amplitude. The effect of considering other neighbors can be taken into account by using the extended tight-binding method (ETB), where the tight-binding parameters dependence on the interatomic distance was obtained from density functional theory.[10] Furthermore, the effect of multiple scattering processes can be taken into account by considering a T matrix.

In §2 we briefly describe the T matrix formalism in

the scattering theory and then introduce the scattering potential for the armchair edged graphene nanoribbon. Also in §2, we show the calculated results for the elastic scattering amplitude within the ETB method, which is compared with the previous STB models. In §3 we introduce the model used for the D band Raman intensity calculation and in §4 we discuss the calculated results of the D band intensity as a function of $E_{\rm laser}$, the nanoribbon width and on the incident and scattered light polarizations. Finally, in §5 a summary of the present calculation is given.

2. THEORETICAL BACKGROUND

Within scattering theory, an elastic scattering amplitude between the initial (i) and final (f) states of the unperturbed system due to an arbitrary perturbation is given as

$$S_{f\leftarrow i} = \delta_{fi} - 2\pi\delta(E_f - E_i)T_{fi}(E) \qquad (1)$$

where the first kronecker delta function (δ_{fi}) becomes unity for identical initial (i) and final (f) states, and the second delta function corresponds to the conservation of energy. The T-matrix, $T_{fi}(E)$, can be calculated in terms of the T operator which can be expressed in terms of Green's function for the perturbed system, $G(E) = (E - H)^{-1}$, as

$$T(E) = V + VG(E)V, \qquad (2)$$

where $H = H_0 + V$ is the perturbed Hamiltonian (graphene ribbon with edges), H_0 is the unperturbed Hamiltonian (infinite graphene sheet) and V is the scattering potential associated with the edge.

The T operator can also be expressed by an unperturbed Green's function $G_0(E) = (E - H_0)^{-1}$ as the following series expansion:

$$T(E) = V + VG_0(E)V + VG_0(E)VG_0(E)V + ... \qquad (3)$$

Each of the terms in the series expansion can be interpreted as processes with a fixed number of scattering events. There are several difficulties related to using the method given by the expansion of Eq.(3). The first difficulty is the fact that for most scattering potentials it is not possible to know *a priori* how fast the series converges and thus the series is usually truncated at a finite number of scattering processes.

Such difficulty is avoided if the Hamiltonian H for the perturbed system can be diagonalized, so that $G(E)$ is expanded in terms of its eigenfunctions, and then the T matrix can be obtained explicitly. This formalism takes into consideration all the possible scattering events and does not depend on the convergence of the series. However, there is a requirement that the eigenfunctions and eigenenergies of the perturbed system must be known in order to allow for the calculation of the T matrix.

In the present work we will apply the T matrix formalism to calculate the scattering amplitude for armchair edges in graphene (the choice of the armchair edges is based on the fact that purely zigzag edges will not contribute to the D band Raman scattering).[11] To calculate the scattering matrix elements $T(E)$ in Eq.(2) for the case of armchair-edged graphene ribbons, the super-cell shown in Fig. 1(a) is considered. The ribbon width L is given by the number of *4 atom* unit cells (shown by a rectangle in the figure) used to construct the super-cell (N_y). Figure 1(b) shows the real space structure of graphene where the *4 atom* unit cell mentioned above is depicted by a light blue (Color Online) rectangle. The graphene reciprocal space structure is shown in Fig. 1(c), where the Brillouin zone corresponding to the *4 atom* unit cell in (b) is also shown in a light gray rectangle. In order to calculate the electronic properties of graphene, it is sufficient to consider only the wavevectors which are within the dark gray area shown in Fig. 1(c). We are mainly interested in the T matrix for large values of L for which we can disregard quantum confinement effects.

2.1. Calculation of the scattering amplitude

The electronic structure of both the graphene ribbon and the infinite graphene layer can be calculated using an extended tight-binding method, where several nearest neighbor interactions are taken into account. For both an infinite graphene sheet and a graphene ribbon, the wavefunctions can be written by considering a unit cell consisting of $2N$ carbon atoms as

$$\psi^b(\vec{k}, r) = \sum_l C_l^b(\vec{k}) \frac{1}{\sqrt{U}} \sum_u \exp(-i\vec{k}\cdot\vec{R}_{ul})\varphi(\vec{r} - \vec{R}_{ul}), \qquad (4)$$

where $C_l^b(\vec{k})$ is the coefficient of the Bloch function, and $\varphi(\vec{r} - \vec{R}_{ul})$ is the atomic orbital at the l-th atom of the u-th supercell. Here l and u go over 2N atomic sites in a unit cell and over all U unit cells in the lattice. The infinite graphene plane is obtained by making $U \to \infty$ and $2N \to \infty$. The Hamiltonian matrix for ψ^b is written in terms of tight-binding wavefunctions as

$$\langle\psi^b(\vec{k}, r)|H_0|\psi^b(\vec{k}, r)\rangle = \sum_{l'l} C_{l'}^{b*}(\vec{k}) C_l^b(\vec{k}) H_{l'l}^0(\vec{k}), \qquad (5)$$

where $H_{l'l}^0(\vec{k})$ is given by

$$H_{l'l}^0(\vec{k}) = \sum_u \exp[i\vec{k}\cdot(\vec{R}_{ul} - \vec{R}_{u'l'})] H_{uu'll'}^0, \qquad (6)$$

where

$$H_{uu'll'}^0 = \langle\varphi(\vec{r} - \vec{R}_{ul})|H_0|\varphi(\vec{r} - \vec{R}_{u'l'})\rangle, \qquad (7)$$

are the atomic matrix elements. The values for the atomic matrix elements and for the overlap parameter

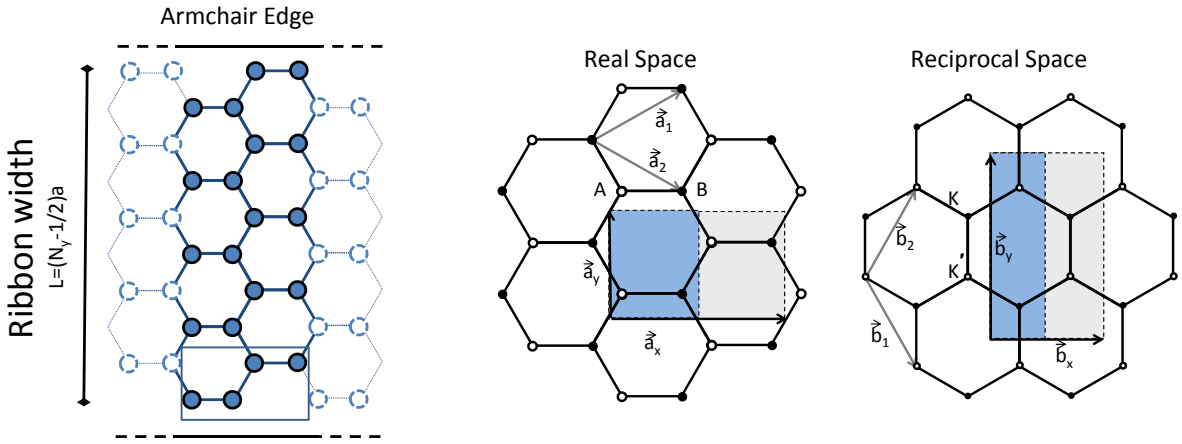

FIG. 1: (Color online)(a) Schematics of a graphene ribbon unit cell for $N_y = 5$, corresponding to $L \sim 1.1$ nm. The filled symbols represent the atoms in the ribbon unit cell, while the open symbols represent adjacent unit cells in the x direction. The box shows a 4 atom unit cell which is used to generate the graphene ribbon. (b) and (c) show, respectively, the real and reciprocal space structures of graphene, highlighting the 4 atom unit cell and its corresponding Brillouin zone.

($S^0_{uu'll'}$), defined as

$$S^0_{uu'll'} = \langle \varphi(\vec{r} - \vec{R}_{ul}) | \varphi(\vec{r} - \vec{R}_{u'l'}) \rangle, \tag{8}$$

were obtained from the DFT calculations of Porezag *et al.*[10]. A cutoff radius of $10a_0 \sim 0.53$ nm (where a_0 is the Bohr radius) is used for the calculation of $H^0_{uu'll'}$ and $S^0_{uu'll'}$ parameters in order to save computation time, which corresponds to considering interactions of up to the seventh nearest neighbors. This choice of parameters has been shown to reproduce well the electronic properties of graphene and single-wall carbon nanotubes.[12]

For the graphene ribbon, we set to zero the values of $H^0_{uu'll'}$ and $S^0_{uu'll'}$ between atoms in the edge and missing atomic positions outside of the edge. Then we can define the single scattering amplitude between two eigenfunctions ($\langle \psi^{b'}(\vec{k}', r) | V | \psi^b(\vec{k}, r) \rangle$, where V denotes the potential change at the edges relative to a bulk atomic site), as

$$\langle \psi^{b'}(\vec{k}', r) | V | \psi^b(\vec{k}, r) \rangle = \sum_{dl} C^{b*}_d(\vec{k}) C^b_l(\vec{k}) V_{dl}(\vec{k}', \vec{k}) \tag{9}$$

and

$$V_{dl}(\vec{k}', \vec{k}) = \sum_u \exp(i\vec{k}\cdot\vec{R}_{ul} - i\vec{k}'\cdot\vec{R}_{u'd}) H^0_{uu'ld} \delta(\vec{k} - \vec{k}' + \vec{Q}), \tag{10}$$

where d represents a missing atom position outside the edge. The vector $\vec{Q}$ in Eq.(10) represents the reciprocal lattice vectors for the super-cell, and the delta function in Eq.(10) represents the conservation of momentum.

Since both the perturbed and unperturbed Hamiltonians are defined for the same unit cell, the wavefunctions of the graphene ribbon $\phi^n(k, r)$ will also be written in terms of the same atomic orbitals as those of the unperturbed graphene structure, but having different tight-binding coefficients $P^n_l(k)$ such that

$$\phi^n(k, r) = \sum_l P^n_l(k) \frac{1}{\sqrt{U}} \sum_u \exp(-ikR_{ul}) \varphi(r - R_{ul}), \tag{11}$$

which can be obtained by diagonalizing the Hamiltonian for the graphene ribbon. Since the electronic states in the graphene ribbon are confined by the edges, the coefficents $P^n_l(k)$ are defined only for k values along the direction of the edges, while when writing the $C^b_l(\vec{k})$ coefficients for the infinite graphene sheet we note that the vector $\vec{k}$ is defined in a two dimensional reciprocal space.

The complete T matrix $\langle \psi^{b'}(\vec{k}', r) | T(E) | \psi^b(\vec{k}, r) \rangle$ can be obtained from Eq. (2) by expanding $G(E)$ in terms of the eigenfunctions of the graphene ribbon $|\phi^n(k, r)\rangle$ which results in the following equation:

$$T_{fi}(E) = V_{fi} + \frac{\Omega_{fn}\Omega_{ni}}{E - E_n + i\epsilon} \tag{12}$$

where T_{fi} is the total scattering amplitude between the initial (i) and final (f) pristine graphene states

$$T_{fi}(E) = \langle \psi^b_f(\vec{k}_f, r) | T(E) | \psi^b_i(\vec{k}_i, r) \rangle, \tag{13}$$

V_{fi} is the value of the 1^{st} Born approximation term

$$V_{fi} = \langle \psi^{b_f}(\vec{k}_f, r)|V|\psi^{b_i}(\vec{k}_i, r)\rangle, \tag{14}$$

and

$$\Omega_{ni} = \langle \phi^{n}(k, r)|V|\psi^{b_i}(\vec{k}_i, r)\rangle \tag{15}$$

is the matrix element for the scattering between the i-th state to an n-th eigenstate ($\phi^n(k,r)$) of the graphene ribbon. Similarly

$$\Omega_{fn} = \langle \psi^{b_f}(\vec{k}_f, r)|V|\phi^{n}(k, r)\rangle \tag{16}$$

is the matrix element for the scattering from this same eigenstate n of the graphene ribbon to a final state f. The broadening factor ϵ appears in Eq.(12) in order to remove the singularity in the denominator of this equation and is related to the timescale of the electron-defect interaction.

3. THE D BAND RAMAN INTENSITY CALCULATION

After calculating the elastic scattering matrix elements, it is possible to calculate the D band Raman intensity. According to the work of Martin and Falicov[13] the differential cross-section for the Raman scattering process is given by

$$\frac{d\sigma}{d\Omega} = \frac{\epsilon_0^2 V^2 E_e^2}{4\pi^2\hbar^4 c^4}|K_{ea}^{\lambda,\lambda'}(E_a, E_e)|^2, \tag{17}$$

where E_a and E_e are the energies of the incident (absorbed) and scattered (emitted) photons with λ and λ' polarizations, respectively. Ω is the solid angle for the collection of the scattered light and ϵ_0 is the vacuum permittivity, c is the speed of light and V is the quantization volume for the irradiated field. According to the model for a double resonance Raman process[6,7] the value of the kernel $K_{ea}^{\lambda,\lambda'}(E_a, E_e)$ can be obtained as

$$\left|K_{ea}^{\lambda,\lambda'}(E_a, E_e)\right|^2 = \sum_i \left| \sum_f \frac{M_a^{\lambda}(\vec{k}_i) M_{\rm ep}^{c}(\vec{k}_i, \vec{k}_f) M_{\rm elas}^{c}(\vec{k}_f, \vec{k}_i) M_e^{\lambda'}(\vec{k}_i)}{(\Delta E_{k_i} + i\gamma)(E_{\vec{k}_i}^c - E_{\vec{k}_f}^c - \hbar\omega_{ph} + i\gamma)(E_{\vec{k}_f}^c - E_{\vec{k}_i}^c + i\gamma)} \right|^2, \tag{18}$$

where

$$\Delta E_{\vec{k}_i} = E_a - (E_{\vec{k}_i}^c - E_{\vec{k}_i}^v), \tag{19}$$

and

$$\hbar\omega_{ph} = E_a - E_e, \tag{20}$$

For the matrix elements $M_{\rm ep}^c$, which correspond to the electron-phonon matrix elements for electrons in the conduction (c) band, we have used the previously calculated expression by Jiang *et al.*[14]. The factor γ was considered to be equal to 0.06 eV for all the processes, which corresponds to the assumption that the timescale of the Raman process is mainly governed by the lifetime of electrons due to the electron-phonon interaction[15]. This assumption is only valid for a low density of elastic scattering centers, for which the mean distance between the scattering centers is well below the mean-free path for electron-phonon scattering processes. Using the uncertainty relation for 0.06 eV and the Fermi velocity of graphene 10^6 m/s, we roughly estimate the value of this low density of elastic scattering centers as $n = 10^{11}/\text{cm}^2$ and by assuming the effective cross section for elastic scattering in the two dimensional system to be of the order of $\sigma = 1.0$ nm. This value is consistent with the experiment by Lucchese et al.[16] in which the D-band spectral width changes when the scattering densities increase and reach values of around 10^{12} $1/\text{cm}^2$. Formally, the value of γ due to the electron-phonon scattering should also depend on the laser excitation energy and on the density of defects. However, for simplicity, a constant value for γ is considered in this work. Further studies of how electron-phonon related resonance broadening effects change the laser excitation energy and crystallite size dependence of the D band intensity should be the subject of future work. For the calculations shown in this paper we chose a particular process for which the defect scattering takes place between initial and final states in the conduction band. Other processes involving hole scattering are also possible, and similar results are obtained (not shown here) by considering hole scattering processes. The matrix elements M_a^{λ} and $M_e^{\lambda'}$ correspond to the light absorption and light emission matrix elements, respectively.[17] In such a Raman process it is expected that a stimulated absorption of the photons

takes place while the emission should be usually spontaneous, such that the matrix elements for the absorption and emission are, respectively[18]:

$$M_a^{\lambda}(k) = i\frac{e\hbar}{mE_a}\sqrt{\frac{I}{\epsilon_0 c}}\vec{P}^{\lambda}\cdot\vec{D}(k), \tag{21}$$

and

$$M_e^{\lambda'}(k) = i\frac{e\hbar}{mE_e}\sqrt{\frac{E_e}{2\pi\epsilon_0}}\vec{P}^{\lambda'}\cdot\vec{D}(\vec{k}), \tag{22}$$

where P^{λ} and $P^{\lambda'}$ are the polarization vectors, I is the intensity of the incident beam and the dipolar vector $D(\vec{k})$ is given, within the dipolar approximation ($\exp(ika) \sim 1$) by[17]

$$\vec{D}(\vec{k}) = \langle\psi^c(\vec{k})|\vec{\nabla}|\psi^v(\vec{k})\rangle. \tag{23}$$

To evaluate the importance of considering the long range scattering potential and the effect of the multiple scattering processes on the D band intensity calculation, the electron-defect matrix element ($M_{\rm elas}$) in Eq. (18) was calculated in three different ways:

(1) STB - the simple tight-binding is used for the scattering potential, for which only the 1st nearest neighbor interaction is taken into account. Also, only single scattering processes (1^{st} Born approximation) are considered.

(2) ETB-s - the long-range scattering potential is taken into account using the extended tight-binding model. However only single scattering processes are considered

(3) ETB-m - both the long-range interactions and multiple scattering processes are taken into account.

To calculate the Raman scattering cross section a full calculation was performed for initial and final states in a 256 x 256 mesh of points centered at the K and K' points, respectively, and spanning a $10\pi/6\sqrt{3}a$ x $10\pi/6\sqrt{3}a$ area of the Brillouin zone. For the STB based calculation, the defect scattering matrix element was obtained directly from the expression derived by Sato *et al.*[9]. For the ETB-s and ETB-m models, the defect matrix element for some given k states were obtained by a linear interpolation of the calculated T matrix in each case. The same set of initial and final points were used for all the three models.

4. RESULTS

4.1. Full T matrix calculations

In order to calculate the T matrix (Eq.(12)) we adopt a finite value for ϵ to account for the uncertainty of the energy during the scattering process. To verify that our choice of ϵ is physically sound, we note that it is expected that small variations of ϵ should not change the calculated value for the T matrix significantly. Figure 2 shows the calculated values for the $T_{kk'}$ matrix elements as a function of ϵ for a graphene ribbon with $N_y = 16$ ($\sim$ 0.38 nm). The value for the T matrix shown in Fig. 2 was calculated for $k = 0.86\pi/a$ and $k' = -0.86\pi/a$ ($a = \sqrt{3}a_{cc} = 2.460$ Å) electronic states in either the valence band (shown as blue squares) or the conduction band (shown as red circles).

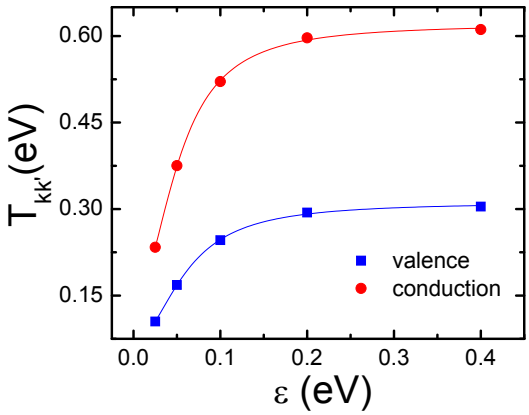

FIG. 2: Dependence of the scattering amplitude $T_{kk'}$ for $k = 0.86\pi/a$ and $k' = -0.86\pi/a$ on the broadening factor ϵ. Squares (circles) are for scattering within the valence (conduction) band. In both cases the T matrix converges for $\epsilon > 0.4$ eV.

In Fig. 2 it can be seen that, for both the valence and the conduction bands, the value of $T_{kk'}$ converged for $\epsilon > 0.4$ eV. The value of $\epsilon = 0.4$ eV was then used to calculate the T matrix for all possible scattering amplitudes for the $N_y = 16$ graphene ribbon. The value of ϵ for which the T matrix converges was found to decrease with increasing ribbon size following a $\epsilon = 6.4/N_y$ eV power law. This dependence is of the same order of magnitude as the value $\epsilon = \hbar v_F/L \sim 16.6/N_y$ eV, which represents the value for ϵ for which those electrons that are scattered by one of the edges are not scattered by the other edge within the time $t \sim \hbar/\epsilon$, in which $v_F \sim 10^6$ m/s denotes the Fermi velocity. The validity of this power law was explicitly verified in the present work for graphene ribbons ranging from $N_y = 8$ to $N_y = 64$.

In Fig. 3(a) we plot the absolute value of $T_{kk'}$ for different nanoribbon widths ranging from $\sim$2 nm (N_y=8) to $\sim$20 nm (N_y=80). The left and right panels of Fig. 3(a) show $T_{kk'}$ for two different initial states k_y, one along the $K\Gamma$, which only scatters towards the opposite $K\Gamma$ direction (left panel) and one along the KM direction, which correspondingly only scatters to the opposite KM direction (right panel). The values of k'_y vary along the $k_x = 0$ line which crosses the center of the Brillouin zone. It can be clearly seen that as the graphene ribbon width increases, the shape of the T matrix converges to a single curve, indicating that for $N_y > 64$ (corresponding to a $\sim$17 nm wide nanoribbon), the confinement effects can be disregarded and the scattering amplitude can be inter-

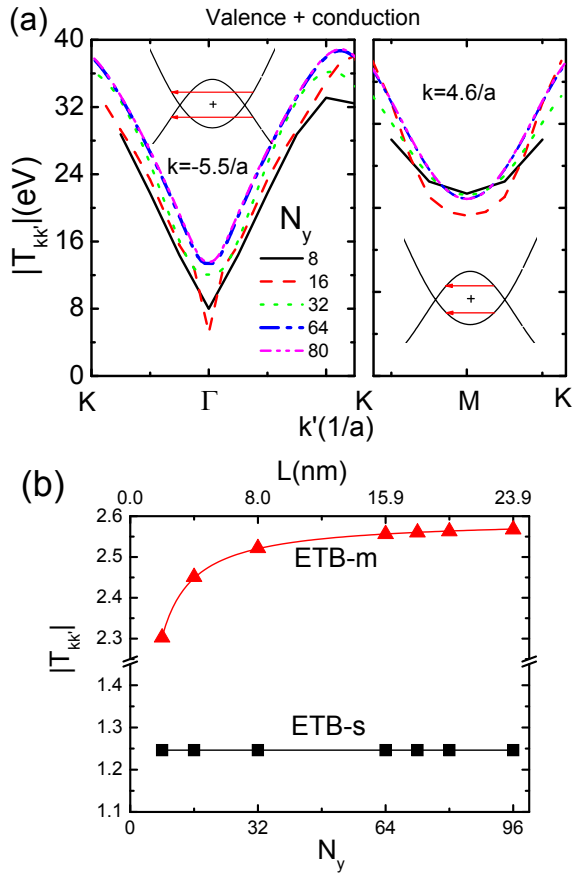

FIG. 3: (a) Comparison between the T matrix calculated for different nanoribbon sizes (number of atoms varying between 32 and 320) for an initial state $k = (0, -5.5/a)$) and final states in the $K\Gamma$ direction (left) and for an initial state, $k = (0, 4.6/a)$) and final states in the KM direction (right). (b) Dependence of the normalized single scattering (square) and multiple (triangles) matrix elements on the nanoribbon width L (N_y).

preted as coming only from the edge scattering. For this reason, for most of the following discussion on the D band intensity, the T matrix was calculated using $N_y = 96$, in order to guarantee a minimum effect of quantum confinement. In Fig. 3(b) we show the absolute value of $T_{kk'}$ for a particular set of initial and final states ($k_x = k'_x = 0$ and $k_y = -k'_y = 0.86\pi/a$) as a function of the nanoribbon width for the single (ETB-s) and multiple scattering (ETB-m) models. It can be clearly seen that for the ETB-m model, the value of the T-matrix converges to a constant value. On the other hand, it is interesting to comment on the effects of the confinement on the scattering amplitude. Within multiple scattering theory, one expects that as the ribbon width decreases, the probability that the electron is consecutively scattered by the two edges should increase, thus affecting the final scattering rate. In this sense, it can be seen in Fig. 3 that the T matrix decreases with decreasing nanoribbon widths. It is possible to understand this effect by noting that we are taking into consideration a backscattering process, for which the wavevectors of the initial and final states have opposite signs. The effect of the two edges regarding the second order process can be interpreted as consecutive scatterings of the electron from each of the edges. Since the two edges are on opposite sides of each other, it is not possible for the electron to undergo two backscattering processes and still end up with a wavevector of the opposite sign, and thus the probability of having a backscattering process should thus be reduced due to the presence of the two edges. In Fig. 3(b) we also show the same plot for the scattering amplitude calculated within the 1st Born approximation. In this case, as the multiple scattering effect is not taken into account, the scattering amplitude does not change with decreasing ribbon width. We should point out that this effect is not caused by the amorphization of the graphene ribbon edges nor by the creation of sp^3 bonding, as suggested by Jorio *et al.*[19] or by Ferrari and Robertson[20], respectively, but to the destructive interference between the multiple scattering processes involving the two edges. However, the experimental observation of this effect should present several challenges, including the difficulty of obtaining perfectly edged graphene ribbons and the fact that for ribbons which are much larger than the mean free path of the electron due to the electron-phonon interaction, the multiple scattering effects involving the two edges will be strongly suppressed. One possible option is to perform the experiment at low temperatures.

4.2. D Band intensity Calculation

Figure 4(a) shows the calculated Raman spectra for different excitation energies. Two characteristic behaviors can be observed as the laser excitation energy is increased: The frequency of the D band increases, while the overall intensity remains fairly constant as $E_{\rm laser}$ increases. The D band frequency dependence is well known to be a consequence of the resonance selection of particular states near the K point. To better probe the laser energy dependence of the D band intensity and to evaluate the effect of long range and multiple scattering effects to the D band intensity we show in Fig. 4(b) the calculated D band intensity as a function of the laser excitation energy for the STB (green circles), ETB-s (black squares) and ETB-m (red triangle) models. It can be seen that the D band intensity remains almost constant within this energy range. A more detailed analysis shows that for the ETB-m and ETB-s models, there is a weak linear dependence which, however, is very small compared to the overall intensity and would thus be very difficult to observe experimentally. For a better comparison with experiments, we also show in Fig. 4(c) the expected value for the I_D/I_G intensity ratio (logarithimic scale) dependence on the excitation laser energy. Since the calculation of the G band intensity dependence on the laser

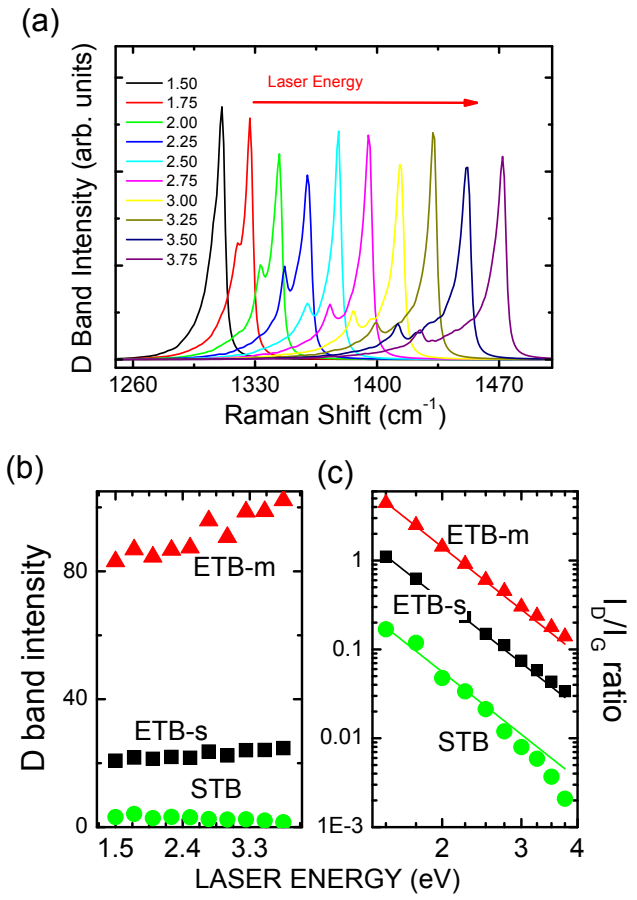

FIG. 4: (a) Laser Excitation Energy dependence of the D-band Raman spectra for the ETB-m model. Dependence of (b) the D band integrated intensity and (c) I_D/I_G ratio on the laser excitation energy (logarithmic scale). The lines are a guide to the eyes showing the expected $E_{\rm laser}^{-4}$ dependence.

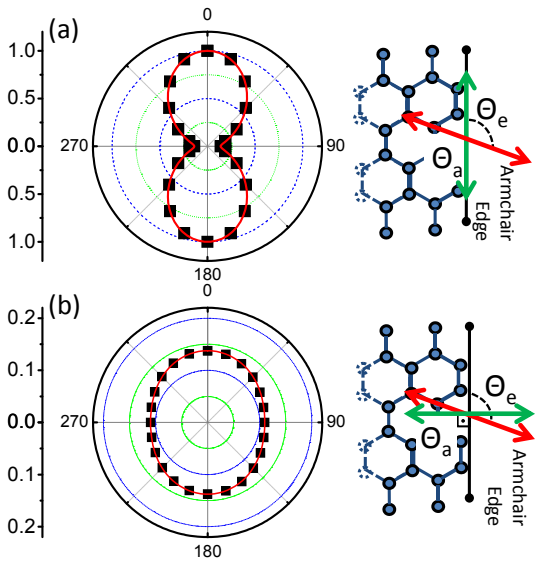

FIG. 5: (Color Online) Dependence of the calculated D band intensity on the scattered light polarization (Θ_e) for (a) $\Theta_a = 0$ and (b) $\Theta_a = 90$. The polarization scheme is shown for each case. The green arrow represents the direction of Θ_a.

excitation energy is still not well established in the literature, we considered the I_G to be given by $I_G \propto E_{\rm laser}^4$, and adjusted the values so that the calculated I_D/I_G ratio for the ETB-m model fits the expected dependence for a ∼50 nm crystallite sized nanographite[3]. The solid lines show the expected $I_D/I_G = AE_{\rm laser}^{-4}$ dependence, indicating that for the ETB-s and ETB-m models, the calculated results are in good agreement with the experimental results.[3,4] It is important to note that, although this $E_{\rm laser}^4$ behavior is well known for non-resonant Raman scattering, the G band Raman process involves resonant electronic states, and thus the $E_{\rm laser}$ dependence of the G band intensity should deviate from this behavior. This point has been discussed in the literature by D. M. Basko[21] where he concludes that for very low excitation energies ($E_{\rm laser} << 3eV$) the G band should follow a $E_{\rm laser}^2$. This different G band intensity behavior would change the I_D/I_G ratio evaluation performed in the present work. Also, recent experimental work indicates that both the D and G band intensities behave differently for graphene and graphite as a function of the laser excitation energy.[4] Further experiments on graphene nanoribbon edges and G band intensity calculations for graphene ribbons are needed in order to improve our understanding of this effect. It is important to comment on the fact that in our calculations, we have assumed spontaneous photon emission, which is a reasonable assumption for the low laser power regime used in Ref.[3]. For higher laser powers it is possible that a stimulated emission process may take place,[22] which should have an altogether different laser excitation dependence. Also, we would like to point out that when comparing the ETB-s and ETB-m models, there is little change in the energy dependence of the D band intensity and I_D/I_G ratio calculation, indicating that for large ribbons, the main effect of considering multiple scattering processes is an overall increase in the D band intensity by a factor of 4. In the case of the STB model, the D band intensity does not show a weak linear dependence on $E_{\rm laser}$, being mostly constant throughout this energy range. However, this difference between the STB and the ETB models has little effect on the I_D/I_G ratio dependence on $E_{\rm laser}$, which is dominated by the fact that I_G increases rapidly with the excitation laser energy. Another important point is that the electron-phonon interaction is expected to increase for higher laser excitation energies, and this should cause a change to the electron-phonon lifetime and consequently to the value of γ thereby adding an extra effect to the dependence of both the D band intensity and the I_D/I_G ratio on $E_{\rm laser}$. This effect has not been taken into account in the present calculation and should be the focus of further studies.

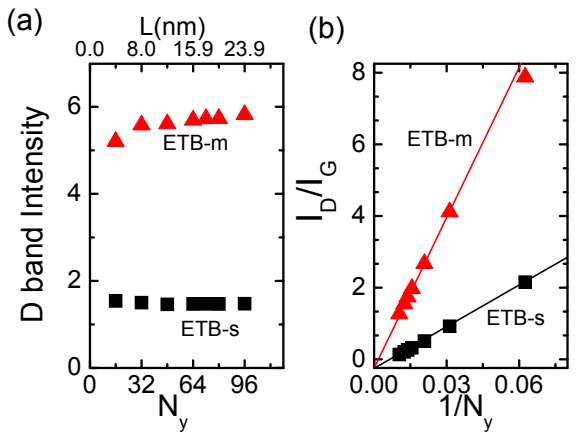

FIG. 6: (Color online) Dependence of (a) the D band intensity on the nanoribbon width N_y and of (b) the I_D/I_G ratio on the inverse nanoribbon width ($1/N_y$) for the ETB-s (squares) and ETB-m (triangle) models for $E_{\rm laser} = 2.0$ eV. The solid lines are a guide to the eye showing the expected $1/N_y$ dependence of the I_D/I_G ratio.

We have also investigated the dependence of the D band intensity on the polarization of the incident and the scattered light with respect to the orientation of the edge. The calculated results can be well described by the following equation

$$I = I_0[\cos^2\Theta_a\cos^2\Theta_e + 0.14\sin(\Theta_a+\Theta_e) + +0.11\sin^2(\Theta_a)\sin^2(\Theta_e)], \quad (24)$$

where I_0 is the maximum intensity and Θ_a and Θ_e are the angles between the direction parallel to the edge and the absorbed and emitted light polarization, respectively. It can be seen that the leading term shows a $\cos^2\Theta_a\cos^2\Theta_e$ dependence, as predicted by Sasaki *et al.*[5]. In Fig. 5(a) and (b), we show the intensity dependence on the polarization of the scattered light (Θ_e in polar coordinates for $\Theta_a = 0^o$ and $\Theta_a = 90^o$, respectively). It can be seen that for $\Theta_a = 90^o$ the D band intensity is almost independent of Θ_e and about 10 times weaker than the intensity for $\Theta_a = \Theta_e = 0^o$. This result is in good agreement with the experimental results of Cong *et al.*[23] who obtained a ratio of 0.2 between the maximum value ($\Theta_a = 0^o$ and Θ_e unpolarized) and the minimum value ($\Theta_a = 90^o$ and Θ_e unpolarized) of the D band intensity.[23]

Finally, in Fig. 6(a) we show the D band intensity dependence on the nanoribbon width ($E_{\rm laser} = 2.0$ eV). For comparison, we show the results obtained using the ETB-s (black square) and ETB-m (red triangle) models. For the ETB-m model the D band intensity seems to be independent of the ribbon width for $N_y > 64$. For such large ribbon widths the two edges act as independent scattering centers, and thus the scattering amplitude is independent of the width. In this regime, the D band intensity is localized in the nanoribbon edges and its localization is dominated by the phase coherent length.[24] For thinner nanoribbons, multiple scattering processes involving the opposite edges become increasingly important, causing a decrease in the D band intensity, as explained above. In the case of the ETB-s model, the D band intensity is independent of the nanoribbon width since it disregards the multiple scattering processes. In order to allow for a comparison with experiments, we also show in Fig. 6(b) the expected I_D/I_G ratio by taking into consideration that the D band intensity is proportional to the ribbon length, while the G band intensity is proportional to the total ribbon area, thus leading to an I_D/I_G ratio which is proportional to $1/N_y$. Once more, we scaled the I_D/I_G ratio in order to fit the experimental results from Cançado *et al.*[3] In Fig. 6(b), the solid lines are a guide to the eye, showing the expected $1/N_y$ behavior. A deviation of the I_D/I_G ratio from the $1/N_y$ dependence for smaller nanoribbons can be clearly seen for the ETB-m model as a result of the fact that for nanoribbons with widths $L < 17$ nm multiple scattering processes involving both edges start to play an important role in the scattering amplitude. For this reason, the scattering rate ceases to be independent of the nanoribbon size causing a departure from the $1/N_y$ behavior."

5. CONCLUSION

In this work we have studied the calculation of the D band intensity for edge scattering in graphene nanoribbons using three different models for the elastic scattering amplitude. The effect of considering the number of nearest neighbors in the tight-binding model and of multiple scattering processes was analyzed. The D band intensity was shown to be weakly dependent on the laser excitation energy, indicating that the $E_{\rm laser}^{-4}$ dependence observed experimentally for the I_D/I_G ratio is mainly due to changes in the G band intensity, which is in agreement with the latest experiments on nanographite.[3] Also, we have shown that for nanoribbons with a width larger than 17 nm, the D band intensity is independent of the nanoribbon width, which leads to the conclusion that for these ribbons the D band intensity is localized at either of the edges. For smaller nanoribbons, we have shown that multiple scattering processes involving the two opposite edges cause a decrease in the D band intensity. This effect indicates that the I_D/I_G ratio should start decreasing even if the crystalllite sizes are larger than the phonon mean free-path. The dependence of the D band intensity on the polarization of incident and scattered light was also investigated.

Acknowledgments

RS acknowledges support from MEXT grant (No.2024-023). EBB acknowledges support from CNPq and

CAPES. MSD acknowledges support from NSF-DMR 10-04147.

* Electronic address: ebarros@fisica.ufc.br

[1] F. Tuinstra and J. L. Koenig, J. Chem. Phys. **53**, 1126 (1970).

[2] L. Cancado, K. Takai, T. Enoki, M. Endo, Y. Kim, H. Mizusaki, A. Jorio, L. Coelho, R. Magalhaes-Paniago, and M. Pimenta, Appl. Phys. Lett. **88**, 163106 (2006).

[3] L. G. Cançado, A. Jorio, and M. A. Pimenta, Phys. Rev. B **76**, 064304 (2007).

[4] R. Narula, R. Panknin, and S. Reich, Phys. Rev. B **82**, 045418 (2010).

[5] K. Sasaki, K. Wakabayashi, and T. Enoki, Phys. Rev. B **82**, 205407 (2010).

[6] C. Thomsen and S. Reich, Phys. Rev. Lett. **85**, 5214 (2000).

[7] R. Saito, A. Jorio, A. G. Souza Filho, G. Dresselhaus, M. S. Dresselhaus, and M. A. Pimenta, Phys. Rev. Lett. **88**, 027401 (2001).

[8] J. R. Taylor, *Scattering Theory The Quantum Theory of Nonrelativistic Collisions* (Dover, New York, 2000).

[9] K. Sato, R. Saito, Y. Oyama, J. Jiang, L. G. Cançado, M. A. Pimenta, A. Jorio, G. G. Samsonidze, G. Dresselhaus, and M. S. Dresselhaus, Chem. Phys. Lett. **427**, 117 (2006).

[10] D. Porezag, T. Frauenheim, T. Köhler, G. Seifert, and R. Kaschner, Phys. Rev. B **51**, 12947 (1995).

[11] L. G. Cançado, M. A. Pimenta, R. A. Neves, G. Medeiros-Ribeiro, T. Enoki, Y. Kobayashi, K. Takai, K. Fukui, M. S. Dresselhaus, R. Saito, et al., Phys. Rev. Lett. **93**, 047403 (2004).

[12] G. G. Samsonidze, R. Saito, N. Kobayashi, A. Grüneis, J. Jiang, A. Jorio, S. G. Chou, G. Dresselhaus, and M. S. Dresselhaus, Appl. Phys. Lett. **85**, 5703 (2004).

[13] M. Cardona, *Light Scattering in Solids* (Springer-Verlag, Berlin, 1982).

[14] J. Jiang, R. Saito, A. Grüneis, S. G. Chou, G. G. Samsonidze, A. Jorio, G. Dresselhaus, and M. S. Dresselhaus, Phys. Rev. B **71**, 205420 (2005).

[15] M. S. Dresselhaus, G. Dresselhaus, R. Saito, and A. Jorio, Physics Reports **409**, 47 (2005).

[16] M. M Lucchese, F. Stavale, E. H Martins Ferreira, C. Vilani, M. V. O. Moutinho, R. B. Capaz, C. A Achete,and A. Jorio, Carbon **48**, 1592 (2010).

[17] A. Grüneis, R. Saito, G. G. Samsonidze, T. Kimura, M. A. Pimenta, A. Jorio, A. G. Souza Filho, G. Dresselhaus, and M. S. Dresselhaus, Phys. Rev. B **67**, 165402 (2003).

[18] Y. Oyama, R. Saito, K. Sato, J. Jiang, G. G. Samsonidze, A. Gruneis, Y. Miyauchi, S. Maruyama, A. Jorio, G. Dresselhaus, et al., Carbon **44**, 873 (2006).

[19] A. Jorio, M. M. Lucchese, F. Stavale, and C. A. Achete, physica status solidi (b) **246**, 2689 (2009).

[20] A. C. Ferrari and J. Robertson, Phys. Rev. B **61**, 14095 (2000).

[21] D. M. Basko, New Journal of Physics **11**, 095011 (2009).

[22] B. P. Zhang, K. Shimazaki, T. Shiokawa, M. Suzuki, K. Ishibashi, and R. Saito, Applied Physics Letters **88**, 241101 (pages 3) (2006).

[23] C. Cong, T. Yu, and H. Wang, ACS Nano **4**, 3175 (2010).

[24] L. G. Cançado, R. Beams, and N. L., arXiv:0802.3709v1 (unpublished).